Modeling and Simulation of a Parallel Hybrid Electric Regional Aircraft for the Electrified Powertrain Flight Demonstration (EPFD) Program

Gokcin Cinar*, Yu Cai†, Russell K. Denney†, and Dimitri N. Mavris†
†School of Aerospace Engineering
Georgia Institute of Technology, Atlanta, Georgia 30332–0150
*Department of Aerospace Engineering
University of Michigan, Ann Arbor, Michigan 48109-2140
Email: cinar@umich.edu

***Abstract*—This paper presents a parametric modeling and integrated aircraft sizing and synthesis approach for a charge depleting parallel hybrid electric architecture. The developed models are integrated within the baseline thin-haul and regional aircraft. In addition to the physical architecture, different modes of operation enabled by propulsion system electrification are also modeled parametrically. The modes of operation presented in this paper are the peak power shaving, climb power electric boost, in-flight battery recharging, and electric taxi. The sizing of the powertrain and the aircraft are performed within the multidisciplinary analysis and optimization environment, E-PASS. The consideration of the physical system and its operation together provides a holistic approach where the propulsion system and the airframe are designed under an optimized power and energy management strategy. The parametric nature of the work enables the design space exploration for electrification and lays the groundwork for future technology projection and uncertainty quantification studies. The developed capability is generic and can be applied on other aircraft classes. The work is done as part of the Electrified Powertrain Flight Demonstration program.**

I. Introduction

Electrified aircraft propulsion (EAP) is a rapidly emerging, transformative concept, under development by NASA and the aerospace industry for over a decade. It has the potential to significantly reduce, and even fully eliminate fuel consumption and aircraft emissions while allowing for more affordable and quieter flights [1]. However, there are also significant challenges including technological, regulative, and infrastructural barriers associated with this technology [2]. Electrification must prove its viability, feasibility and benefits at smaller commercial aircraft classes, such as thin-haul and regional, before it can penetrate single-aisle and wide-body markets.

NASA is investigating the utilization of flight demonstrations to rapidly mature and transition integrated EAP technologies and associated EAP-based vision systems for introduction into the US fleet no later than 2035. This paper aims to present a technical approach developed for the modeling, integration and sizing of hybrid electric powertrains within the vision systems. In this work, vision systems refer to commercial transport concepts that are expected to enter the U.S. air transportation system in the 2030 to 2035 timeframe.

The work presented in this paper builds on a series of papers given in Ref. [3]–[6]. The previous work explored the design and trade space for a 19-passenger (19-pax) thin-haul and a 50-passenger (50-pax) regional aircraft with EAP [3]. The 19-pax and 50-pax technology reference and baseline models with conventional propulsion systems were built parametrically [4]. This paper describes the modeling of selected hybrid electric propulsion system architectures, their modes of operation, and implementation on the 50-pax EAP system.

II. Electrified Powertrain Architecture

The thin-haul and regional commuters present relatively more short-term opportunities for electrification compared to heavier jets. This work investigates the feasibility and benefit assessment of a charge depleting parallel hybrid electric propulsion architecture on the 50 passenger class EAP vision system. This architecture uses electric machines to supplement the thermal core power of a turbine engine and have the ability to provide a substantial fraction of energy for short range missions in all-electric or hybrid mode. Fig. 1 notionally depicts the integrated electrified powertrain boundary. There are two propellers on this system. During the hybrid electric operation, each propeller is driven by a turboshaft engine and an electric motor. The electric motors are powered by a battery universal battery pack consisting of lithium-ion battery cells. During in-flight charging, the electric motors act as generators and convert the mechanical power on the shaft (generated by the turboshaft engines) to electrical power to charge the battery.

A. Parametric Modeling of the Propulsion Architecture

The development of parametric, physics-based models for all the components shown in Fig. 1 was presented in detail in previous work [3], [7] and will not be further explained in this paper.

The modeling approach for the propulsion architecture and its operation leverages a novel method of categorizing the propulsion system components into three main sources and

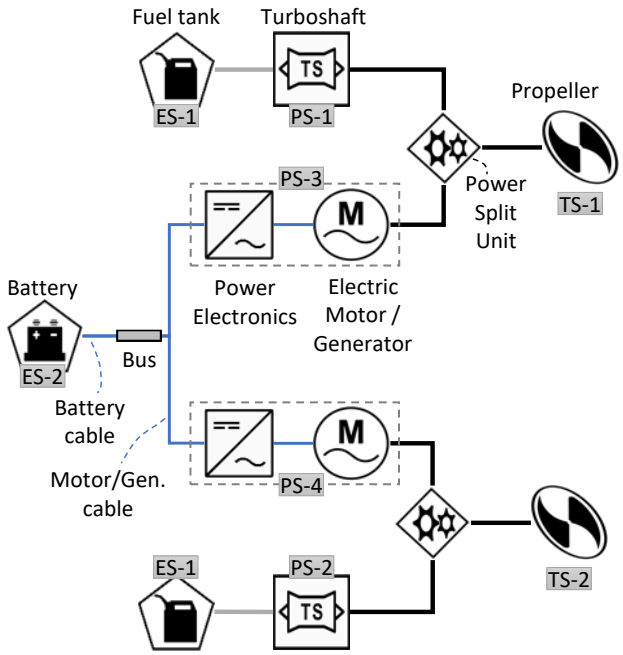

Fig. 1. Integrated electrified powertrain boundary. Main components were grouped as energy sources (ES), power sources (PS), and thrust sources (TS).

establishing their relationships through a set of matrices, as first introduced by Cinar in Ref. [7], [8]. These sources are:

- **Thrust Source (TS):** a subsystem that generates thrust (e.g. propeller, fan)
- **Power Source (PS):** a subsystem that generates primary power (e.g. gas turbine engine, electric motor, generator)
- **Energy Source (ES):** a subsystem that stores energy to be used by the primary power source (e.g. battery, fossil fuel, hydrogen fuel cell)

These three sources can be systematically used to describe any type of propulsion system architecture. In Fig. 1, major components of the parallel hybrid electric architecture were mapped to the three source categories and enumerated by identification numbers. The enumerated sources are used to create the "interdependency matrices," a set of matrices used the describe the physical connection and the power flow during an operation among the three source categories. These matrices are used to lay out the following relationships:

- **Thrust Source - Power Source Matrix (B_{TSPS}):** describes which thrust source(s) is directly connected to which power source(s). E.g. in Fig. 1, propeller (TS-1) is directly connected to the turboshaft engine PS-1 and the electric motor PS-3. A "direct connection" means that a source can be used to drive or power another source without any other sources of the same category in between.
- **Driven Power Source - Driving Power Source Matrix (B_{PSPS}):** If there are multiple power sources on the same power path, this matrix identifies the power sources that are directly connected to other power sources. E.g. in Fig. 1, the turboshaft engine PS-1 drive the generator PS-3 while the battery is being recharged.
- **Power Source - Energy Source (B_{PSES}):** describes which power source(s) gets its energy from which energy source(s). E.g. in Fig. 1, the turboshaft engines PS-1 and PS-2 are connected to the fuel tank ES-1, and the electric motors PS-3 and PS-4 are connected to the battery ES-2.

The interested reader can refer to Ref. [9] for further details and discussions on how to utilize this mathematical framework to describe, build, and operate any type of architecture. Utilizing the framework in Ref. [9], four interdependency matrices, $B_{\infty TS}$, B_{TSPS}, B_{PSPS}, and B_{PSES}, were created to define and operate the parallel hybrid propulsion system architecture model depicted in Fig. 1 as follows:

$$\boldsymbol{B_{TS\infty}} = \begin{bmatrix} \lambda_{\infty,TS1} & \lambda_{\infty,TS2} \end{bmatrix} \tag{1}$$

$$\boldsymbol{B_{TSPS}} = \begin{bmatrix} \lambda_{TS1,PS1} & 0 & \lambda_{TS1,PS3} & 0 \\ 0 & \lambda_{TS2,PS2} & 0 & \lambda_{TS2,PS4} \end{bmatrix} \tag{2}$$

$$\boldsymbol{B_{PSPS}} = \begin{bmatrix} 0 & 0 & 0 & 0 \\ 0 & 0 & 0 & 0 \\ \lambda_{PS3,PS1} & 0 & 0 & 0 \\ 0 & \lambda_{PS4,PS2} & 0 & 0 \end{bmatrix} \tag{3}$$

$$\boldsymbol{B_{PSES}} = \begin{bmatrix} \lambda_{ES1,PS1} & 0 \\ \lambda_{ES1,PS2} & 0 \\ 0 & \lambda_{ES2,PS3} \\ 0 & \lambda_{ES2,PS4} \end{bmatrix} \tag{4}$$

where λ_{XY} is the operational control variable defined for each directly connected source X and Y. It is expressed as the ratio of the power contribution of Source X (P_{XtoY}) to the required or desired power of the upstream Source Y (P_Y), as shown in Eq. 5:

$$\lambda_{XY} = P_{XtoY}/P_Y \tag{5}$$

Note that, by this definition, the sum of λ_{XY} must be equal to 1 for any row of the matrix B_{XY}. Then, new property matrices A_X and A_Y can be defined for sources X and Y such that these property matrices hold information (such as power) of each source within the same source category:

$$\boldsymbol{P_X} = \begin{bmatrix} P_{X1} & P_{X2} & \dots & P_{Xm} \end{bmatrix} \tag{6}$$

$$\boldsymbol{P_Y} = \begin{bmatrix} P_{Y1} & P_{Y2} & \dots & P_{Yn} \end{bmatrix} \tag{7}$$

Finally, the property of each Source X can be proportionally propagated to a connected Source Y through a matrix multiplication with λ_{XY}. In the case of additive properties, such as power, the propagation of power of multiple sources (X1, X2, ..., Xm) driving another source (Y1, Y2, ..., Yn) can be described as:

$$\boldsymbol{A_X} = \boldsymbol{A_Y B_{XY}} \tag{8}$$

The interdependency matrices are used in the mission analysis by calculating the power flow at the upstream and the downstream of every source, as depicted in Fig. 2. As shown in

this figure, the direction of electric power flow path reverses when recharging the battery. The operational control variables are then manipulated throughout the flight mission to change the power management strategy. The most upstream power requirement is the overall required thrust power $(TV)_{req}$, which is a function of drag, and the time rate of change of mechanical energy of the vehicle:

$$(TV)_{req} = DV + \frac{d}{dt}\left(Wh + \frac{1}{2}\frac{W}{g}V^2\right) \tag{9}$$

where D is drag, V is airspeed, t is time, W is weight, h is altitude, and g is the gravitational acceleration. Then, $(TV)_{req}$ is distributed to the thrust sources as defined by $\lambda_{\infty TS}$, where the subscript ∞ denotes the free stream. Then, power required from each source is calculated by going from upstream to downstream using Eqs. 10 through 13 at every time step:

$$\boldsymbol{P_{TS}} = (TV)_{req}\boldsymbol{B_{\infty TS}} \tag{10}$$

$$\boldsymbol{P^*_{PS}} = \boldsymbol{P_{TS}}\boldsymbol{B_{TSPS}} \tag{11}$$

$$\boldsymbol{P_{PS}} = \boldsymbol{P^*_{PS}}\boldsymbol{B_{PSPS}} \tag{12}$$

$$\boldsymbol{P_{ES}} = \boldsymbol{P_{PS}}\boldsymbol{B_{PSES}} \tag{13}$$

where P^*_{PS} in Eq. 11 is the power output of driven power sources; it is an intermediary step in calculating the final total power output of all power sources P_{PS} in Eq. 12.

B. Gas Turbine Engine Model

To optimize the performance of a future hybrid electric aircraft, the turbine engine performance, size and weight should be considered along with the other components of the vehicle. This capability is provided by a "scalable" engine model, which predicts the expected performance and weight of new centerline engine designs over a continuous range of design power levels. The scalable engine model was developed using the NASA Numerical Propulsion System Simulation (NPSS) [10]. Future performance trends were derived from several published sources, notably Refs. [11]–[13]. The engine cycle, defined by the design pressure ratio (OPR) and turbine inlet temperature (T4), is assumed to vary with engine design power. Performance improvements are assumed to be due to evolutionary improvements in component aerodynamics and turbine cooling as well as the incorporation of new technologies such as CMC materials and 3D manufacturing. Turbine cooling flows are estimated using the algorithm developed by Gauntner [14].

A multiple design point (MDP) method [15] is used to couple the top-of-climb power requirement to the sea level calibration point. The three design points are defined as follows:

- Sea level takeoff: calibration point; sets design power, OPR, and T4
- Hot day: engine power is flat-rated to a 95°F day; sets turbine cooling and T4 limit
- Top-of-climb: engine is sized to provide required power at TOC

C. Electric Powertrain Models

In an earlier study, the authors developed parametric, physics-based models for the electric powertrain components shown in Fig. 2. This section provides a brief overview of the modeling assumptions and the interested reader is referred to Ref. [3] for in-depth description for each model.

The parametric, loss-based electric motor model builds up efficiency maps based on Coulomb frictional, windage, iron, copper, and parasitic losses in an electric motor. The power converter model functions as both inverter and rectifier. The model assumes constant efficiency throughout flight. The AC voltage and current are governed by the electric machine, while the DC voltage is dictated by the battery. The power converter weight is calculated based on specific power and peak power. The parametric battery model takes in cell unit information and sizes the pack for high level requirements such as capacity and voltage. The baseline cells were modeled after the Samsung INR18650-30Q cells which are used on the X-57 Maxwell aircraft. The maximum and minimum limits of the battery state of charge are 100% and 20%, respectively. The electric cables were designed via efficiency which is used to determine the resistance and total conductor area. The weight is built up from cable components including the conductors, insulation, magnetic shielding, and cooling jacket, while accounting for void space between components.

III. Electrified Powertrain Operation

The design mission profile of the 50-pax EAP is depicted in . More details of this mission (including the reserve mission profile) was provided in Ref. [4]. This profile was modeled by discretizing each flight segment using mission points. The operational control variables were mapped to each mission point and varied based on the desired power management strategy. This modeling allows for the parametrization of the power management strategy throughout the flight, eliminating the need to make sub-optimal assumptions such as constant hybridization throughout a mission segment.

The following modes of operation were identified and parametrically modeled for the parallel hybrid electric vision systems. The calculations provided in each section are repeated at every mission point of the relevant mission segment(s).

A. Peak power shaving

The turboprop engines of the baseline aircraft were sized for takeoff conditions. In a parallel hybrid electric architecture, the battery and the electric motors can be used to provide partial power during takeoff. This means that under otherwise identical conditions, a smaller engine core with a lower peak power would suffice to maintain the same aircraft takeoff performance. This strategy provides engine weight savings and potentially higher efficiency in cruise fuel burn. [3], [16]. An "electric motor power split" variable, Λ_{em} was defined to control this strategy as the ratio of maximum total electric motor power ($P_{em,max,total}$) to sea level static total power of the aircraft (P_0):

$$\Lambda_{em} = P_{em,max,total}/P_0 \tag{14}$$

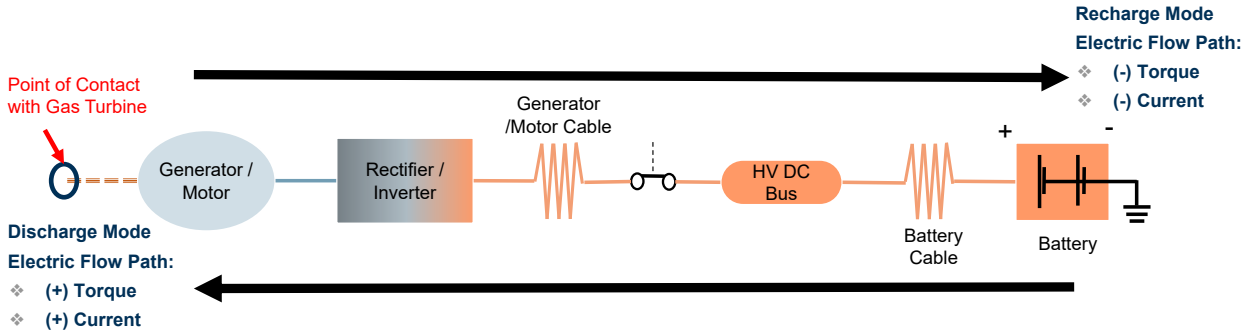

Fig. 2. Electric power flow paths on the electric powertrain during battery discharge and charge modes. The amount and direction of power being propagated depends on the required shaft power and the power management strategy.

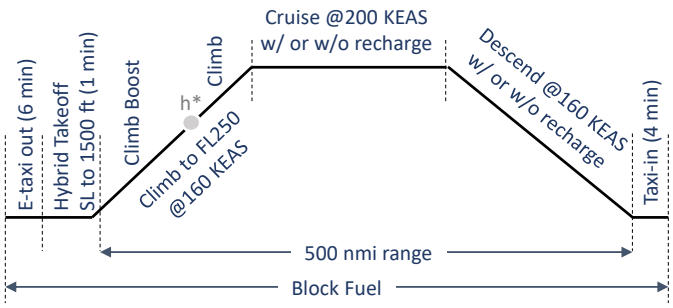

Fig. 3. 50-pax EAP mission profile. Only low altitude climb boost is shown in this figure.

The power split variable is one of the sizing factors for the engine and the electric motor, as described in Section IV-A.

B. Climb power boosting

In this model, the climb segment was parametrically hybridized to assess the impact of the amount, timing, and duration of hybridization as a function of electric motor power and altitude. The duration and amount of the electric boost has a significant impact on the battery size, as they contribute to the required electric energy. Thus, this approach aims to optimize the electrification strategy for the design mission during the aircraft sizing process. The model is initialized by the selection of low or high altitude electric boost (*lo-alt* and *hi-alt*). The user also specifies the threshold altitude h^* after which the electrification starts (hi-alt) or stops (lo-alt). The electric motor power during climb is determined by the electric motor power code (PC_{em}) as defined in Eq. 17. During climb, the turboshaft engines were set to run at their max power available which is a function of altitude (h), Mach number (M), and the maximum engine power code ($PC_{engine,max}$). Equations 15-18 describe the climb power boosting model:

$$(TV)_{clb} = \eta_{prop} \sum_{j=1}^{4} P_{PS,j} \tag{15}$$

$$P_{engine} = f_{engine}(h, M, PC_{engine,max}) \tag{16}$$

$$P_{em} = PC_{em}\ P_{em,max} \tag{17}$$

$$PC_{em} = \begin{cases} 0\% < PC_{em} \leq 100\%, & \text{if } h \leq h^* \text{ \& lo-alt} \\ 0\% < PC_{em} \leq 100\%, & \text{if } h \geq h^* \text{ \& hi-alt} \\ 0\%, & \text{otherwise} \end{cases} \tag{18}$$

where $(TV)_{clb}$ is the climb thrust power, η_{prop} is the propeller efficiency, f_{engine} is the turboshaft engine model, and P_{engine} and P_{em} are the output shaft power of the turboshaft engine and the electric motor, respectively. The mission profile in Fig. 3 depicts the lo-alt case.

C. In-flight battery recharging

The battery must have sufficient charge at the beginning of each mission. The design mission analysis made in this study assumes 100% State of Charge (SoC) at the beginning of the mission. The charging capability was included in the powertrain models for cases where the necessary infrastructure to fully charge the battery at the date does not exist or is not viable. During recharging, the direction of power propagation is reversed (as shown in Fig. 2), and the the battery is charged by the gas turbine and the generator (i.e. turbogenerator). The user specifies the charging C-rate, and the generators must meet the charging power demand as allocated by $\boldsymbol{B}_{PSPS}$. The generator power required to charge the battery is calculated in Eq. 13, and added to the shaft power required to drive the thrust sources in Eq.12. An iteration takes place on power source efficiency.

In this application, the two generators provide equal power to charge the battery synchronously. Charging occurs during cruise and/or descent at the same or different rates. The charging C-rate is capped based on the available power in the power sources in the charging power path. Charging stops when the battery state of charge is 100%. Previous work [3] revealed that in-flight brings a substantial fuel burn penalty, thus the powertrain and the aircraft must be designed to provide a net fuel burn benefit even with in-flight charging.

D. E-taxi

The thin haul and regional aircraft are mostly utilized in small airports which typically do not have heavy traffic. This results in relatively short taxi in and out times compared to larger transports, such as the 4 minute taxi allowance quoted by the ATR-42 brochure [17]. However, fuel burned during

taxi is still significant and the resulting emissions contribute to local air pollution at airports. The electric motors are also highly efficient at a wide range of torque and speed conditions, as opposed to the turboprop engine which is much less efficient at low throttle settings. E-taxi operation will be modeled by using one or both of the electric motors in the powertrain to drive the one or both of the propellers and carry out the ground operation through static thrust generated by the propellers. The electric motors can also be used to power other necessary subsystems during taxi. The use of E-taxi imposes a lower bound on the electric motor sizing power, which is computed based on the critical thrust requirement and the propeller performance:

$$T_{\text{taxi}} = mg\mu_{rr} + mg\gamma + ma \tag{19}$$

$$C_T = f_{\text{prop}}(C_P, n) \tag{20}$$

$$T_{\text{taxi}} = C_T \rho n_*^2 D^4 \tag{21}$$

$$P_{\text{taxi}} = C_P \rho n_*^3 D^5 \tag{22}$$

$$n_* = \arg\min_n P_{\text{taxi}} \tag{23}$$

where m is the aircraft gross mass at taxi, conservatively assumed equal to the maximum ramp weight, g is the gravitational acceleration, μ_{rr} is the rolling friction coefficient, γ is the critical uphill slope, a is the critical acceleration, f_{prop} is the propeller model, C_T is the thrust coefficient, C_P is the power coefficient, ρ is the air density, n is the propeller speed, and D is the propeller diameter. Specifically, $\gamma = 0.015$ and a is computed based on a constant acceleration from 0 to 10 kts in 20 sec. In Eq. (23), the propeller speed is allowed to vary below what is required by conventional engine-driven taxi to minimize the shaft power requirement given the thrust requirement.

IV. Integrated Aircraft and Powertrain Sizing and Synthesis

The architecture and powertrain component models were integrated with the 50-pax baseline aircraft model developed in Ref. [4]. All the models, except for the turboshaft model created in NPSSS, were built in a multi-disciplinary analysis and optimization environment called Electrified Propulsion Architecture Sizing and Synthesis (E-PASS), developed by Cinar [8]. E-PASS is a Matlab-based aircraft sizing and synthesis tool that enables the design and performance evaluation of conventional and advanced aircraft concepts with any type of propulsion system architecture. It utilizes the matrix-based approach described in Section II and the parametric modeling of the electrified mission operation described in Section III for the co-design and operation of the aircraft and its powertrain. The building blocks and the sizing loops of E-PASS are depicted in Fig. 4. The sizing processes leveraged in this work were provided in detail in Ref. [3]

A. Sizing of Hybrid Propulsion System

For the parallel hybrid architecture of interest, two top-level parameters characterize the sizing of the propulsion system: 1) PWR, the total power-to-weight ratio of the aircraft at sea-level condition, and 2) Λ_{em}, the fraction of required sea-level power to be supplied by the electric motors. Based on the aircraft gross weight and PWR, the total power required (P_0) from all power sources are first computed. Then, the minimum required rated power of each power source is computed based on λ_{em}:

$$P_{eng,max\ SLS} = \frac{1-\Lambda_{em}}{2} P_0 \tag{24}$$

$$P_{em,max} = \frac{\Lambda_{em}}{2} P_0 \tag{25}$$

Since the electric motors do not drive the propellers in cruise, a few point performance requirements additionally constrain the sizing of the turboshaft engines:

- The two engines must be capable of providing specific excess power of 300 ft/min at cruise altitude at climb speed;
- The two engines must be capable of providing sufficient power to sustain level flight at cruise altitude at cruise speed.

When Λ_{em} is sufficiently large, one of these point performance constraints becomes active, and the engines are upsized accordingly. In this case, the total power available at sea level will be greater than P_0. Similarly, if E-taxi is used and if Λ_{em} is sufficiently small, then the taxi power requirement mentioned in Sec. III-D will dictate the sizing of electric motors.

B. Sizing of the Battery

There are two requirements that determine the size of the battery: total energy and maximum power. First, the amount of energy required from the two energy sources, fuel and battery, is dictated by the operational power management strategy in terms of discharging rate and duration. The battery must have a State of Charge (SoC) of at least 20% after executing: 1) E-taxi, 2) hybrid takeoff, and 3) hybrid climb. As part of the mission analysis, the required battery energy is calculated as a sum of energy required to satisfy these three conditions. If the battery energy is less than the required energy, more cells are added to the battery pack to meet the energy demand.

Secondly, the battery power is a function of the discharge current and system voltage. The maximum discharge current, I_{max}, depends on the cell level characteristics and the number of cells connected in parallel inside the battery pack. If the required current during battery discharge is less than I_{max}, then more cells in parallel are added to the battery pack to meet the power demand.

Battery weight is determined by the cell build-up and weight model.

V. Results

Figure 5 presents the trends for electric motor rated power, battery mass, and vehicle climb performance as a function of climb boost strategy. A low-altitude boost is simulated where the electric motor power setting (PC_{em}) is varied

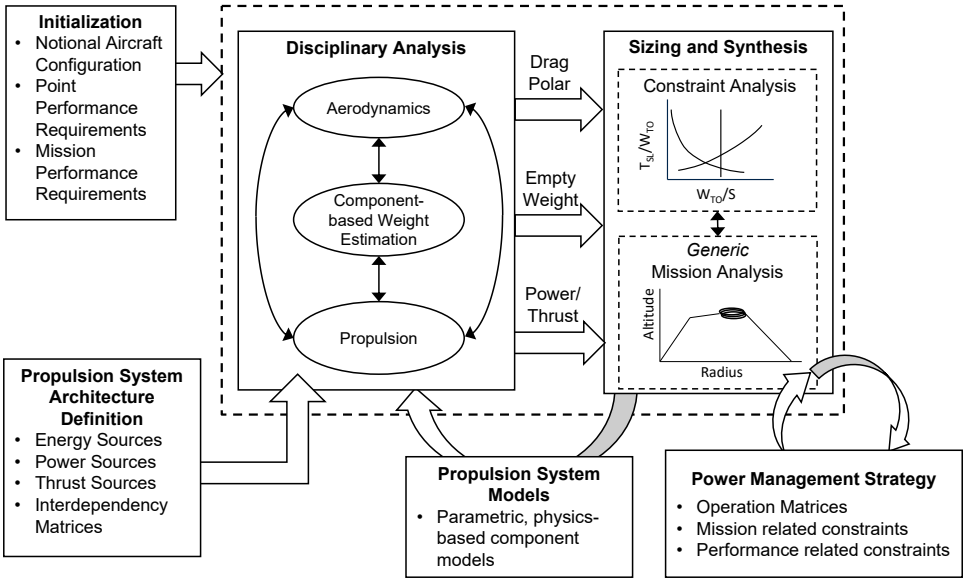

Fig. 4. Building blocks of the modeling and simulation environment: E-PASS.

between 50% and 100% and the electric motor switch-off altitude (h^*) is varied between 12000 and 24000 ft. A constant electric motor power split $\Lambda_{em} = 0.1$ is assumed for all simulations. It can be observed that the battery mass has a lower bound of approximately 115 kg, which is constrained by the maximum current limit at takeoff. As PC_{em} increases, the electric power consumption increases, which ultimately drives the sizing of the battery. Similarly, as h^* increases, the battery energy requirement becomes the driving factor for battery sizing instead of the maximum current limit. As the battery becomes larger and heavier, the vehicle takeoff gross weight becomes higher, which leads to an upsized electric motor.

Figure 5 also shows the trade-off between battery mass and climb performance. With the low-altitude boost stratey, as PC_{em} increases, the sea level rate of climb increases and the time-to-climb decreases due to higher power available; a longer climb boost has negligible impact on the sea level rate of climb, but has a significant impact on time-to-climb. Both improvements in performance come at a cost of larger battery and electric motors.

Figure 6 shows the power requirement and propeller speed for E-taxi with different assumptions of surface slope (γ) and acceleration (a) as mentioned in Eq. (19). It can be seen that, while the power requirement for steady taxi is typically in the range of 10-20 kW for each electric motor, the critical scenario where the aircraft has to achieve an acceleration of $a = 0.5$ kt/sec on an uphill surface for runway crossing imposes a much higher requirement on the rated power of the electric motors, which is approximately four times as much as the steady taxi power. It is also noticed that the optimal propeller speed which minimizes the power requirement during steady taxi is considerably lower than the propeller speed for conventional engine-driven taxi (845 RPM based on Ref. [18]),

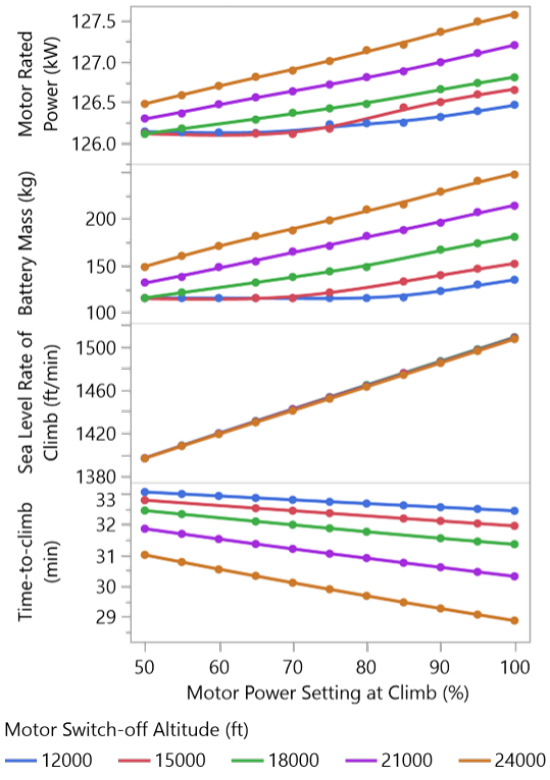

Fig. 5. Sizing of electrified powertrain and vehicle performance for different climb strategies

demonstrating the flexibility and optimality of E-taxi.

VI. Conclusion

Acknowledgment

The authors would like to thank NASA for their support of this effort under AWD-002344 (NIA-602015), especially

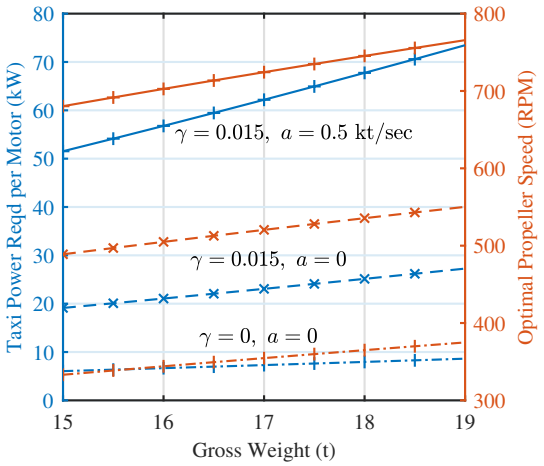

Fig. 6. E-taxi power requirements and optimal propeller speed

Gaudy Bezos-O'Connor, Ralph Janson, and Fayette Collier.

REFERENCES

[1] D. Miranda, "2020 NASA technology taxonomy," 2020.

[2] N. K. Borer, C. L. Nickol, F. Jones, R. Yasky, K. Woodham, J. Fell, B. Litherland, P. Loyselle, A. Provenza, L. Kohlman *et al.*, "Overcoming the adoption barrier to electric flight," in *54th AIAA Aerospace Sciences Meeting*, 2016, p. 1022.

[3] G. Cinar, Y. Cai, M. V. Bendarkar, A. I. Burrell, R. K. Denney, and D. N. Mavris, "System analysis and design space exploration of regional aircraft with electrified powertrains," in *AIAA SCITECH 2022 Forum*, 2022, p. 1994.

[4] Y. Cai, J. Xie, G. Cinar, and D. N. Mavris, "Advanced 2030 turboprop aircraft modeling for the electrified powertrain flight demonstration program," in *2022 IEEE/AIAA Transportation Electrification Conference and Electric Aircraft Technologies Symposium*, Anaheim, CA, June 2022.

[5] C. L. Pastra, C. Hall, G. Cinar, J. Gladin, and D. N. Mavris, "Specific power and efficiency projections of electric machines and circuit protection exploration for aircraft applications," in *2022 IEEE/AIAA Transportation Electrification Conference and Electric Aircraft Technologies Symposium*, Anaheim, CA, June 2022.

[6] C. Hall, C. L. Pastra, A. Burell, J. Gladin, and D. N. Mavris, "Projecting power converter specific power through 2050 for aerospace applications," in *2022 IEEE/AIAA Transportation Electrification Conference and Electric Aircraft Technologies Symposium*, Anaheim, CA, June 2022.

[7] G. Cinar, D. N. Mavris, M. Emeneth, A. Schneegans, and Y. Fefermann, "Development of parametric power generation and distribution subsystem models at the conceptual aircraft design stage," in *55th AIAA Aerospace Sciences Meeting*, 2017, p. 1182.

[8] G. Cinar, "A methodology for dynamic sizing of electric power generation and distribution architectures," Ph.D. dissertation, Georgia Institute of Technology, 2018.

[9] G. Cinar, E. Garcia, and D. N. Mavris, "A framework for electrified propulsion architecture and operation analysis," *Aircraft Engineering and Aerospace Technology*, 2020.

[10] J. K. Lytle, "The numerical propulsion system simulation: An overview," National Aeronautics and Space Administration, Glenn Research Center, Cleveland, OH, Tech. Rep. NASA/TM-2000-209915, June 2000.

[11] C. A. Snyder and M. T. Tong, "Modeling turboshaft engines for the revolutionary vertical lift technology project," in *75th Annual Vertical Flight Society (VFS 2019) Forum and Technology Display, Philadelphia*, 2019.

[12] J. BETTNER, "Component arrangement studies for an 8000 shp turboshaft high technology core," in *26th Joint Propulsion Conference*, 1990, p. 2398.

[13] R. L. Vogt and A. Sehra, "Next generation 2 mw turboshaft and turboprop engines," in *Turbo Expo: Power for Land, Sea, and Air*, vol. 78880. American Society of Mechanical Engineers, 1993, p. V001T01A005.

[14] J. W. Gauntner, "Algorithm for calculating turbine cooling flow and the resulting decrease inturbine efficiency," National Aeronautics and Space Administration, Tech. Rep. NASA/TM-81453, 1980.

[15] J. S. Schutte, "Simultaneous multi-design point approach to gas turbine on-design cycle analysis for aircraft engines," Ph.D. dissertation, Georgia Institute of Technology, 2009.

[16] T. Spierling and C. Lents, "Parallel hybrid propulsion system for a regional turboprop: conceptual design and benefits analysis," in *2019 AIAA/IEEE Electric Aircraft Technologies Symposium (EATS)*. IEEE, 2019, pp. 1–7.

[17] ATR, "ATR-42-600," Brochure, 2015. [Online]. Available: https://skybrary.aero/bookshelf/books/3695.pdf

[18] *Systems*, ATR Product Support & Services, Jun. 2012.